ISSN 0965-5441, Petroleum Chemistry, 2019, Vol. 59, No. 12, pp. 1320–1325. © Pleiades Publishing, Ltd., 2019.
Russian Text © The Author(s), 2019, published in Nanogeterogennyi Kataliz, 2019, Vol. 4, No. 2, pp. 132–137.

Benzene Alkylation with Propylene in the Presence of Nanocrystalline Zeolites BEA with Different Compositions

T. O. Bok[a], E. P. Andriako[a, *], D. O. Bachurina[a], E. E. Knyazeva[a, b], and I. I. Ivanova[a, b]

[a] *Topchiev Institute of Petrochemical Synthesis, Russian Academy of Sciences, Moscow, 119991 Russia*

[b] *Faculty of Chemistry, Moscow State University, Moscow, 119991 Russia*

**e-mail: e.andriako@mail.ru*

Received July 8, 2019; revised July 30, 2019; accepted August 9, 2019

Abstract—The effect of the chemical composition of nanocrystalline zeolites BEA on their physicochemical and catalytic properties in benzene alkylation with propylene is studied. It is shown that a decrease in the Al_2O_3 content in the reaction mixture during the synthesis of nanocrystalline zeolites leads to a decrease in the size of both the primary nanocrystals and their aggregates. The acidic properties of nanocrystalline zeolites BEA correlate with the aluminum concentration in the samples. The high concentration of acid sites of about 1400 μmol/g and the developed surface of zeolites BEA represented by nanocrystal aggregates provide a high activity of the samples and a high selectivity for the target product—cumene—owing to a decrease in the contribution of side reactions, namely, the secondary alkylation and oligomerization of propylene.

Keywords: zeolite BEA, benzene alkylation with propylene, cumene, nanocrystals, acidic properties

DOI: 10.1134/S0965544119120028

Benzene alkylation with propylene is one of the important petrochemical processes, because it provides the production of isopropylbenzene (cumene), which is an intermediate in the synthesis of phenol [1, 2]. Conventional catalysts for the production of cumene are mineral acids and Lewis acids (H_2SO_4, H_3PO_4, $AlCl_3$, etc.) [3]; the use of these acids causes problems associated with the formation and disposal of waste and corrosion of the equipment. In the 1990s, the use of zeolite-based solid acid catalysts provided an efficient implementation of highly environmentally friendly commercial processes for cumene production [4].

The zeolite components of cumene synthesis catalysts are zeolites of the BEA, FAU, MOR, MFI, and MWW framework types [4–7]; among these materials, zeolite BEA is characterized by a higher selectivity for cumene and a lower selectivity for *n*-propylbenzene and propylene oligomers. The specific features of zeolite BEA are associated, on the one hand, with the structural properties of the material: the BEA zeolite structure is formed by a system of pores with a diameter of 0.66 × 0.67 and 0.55 × 0.56 nm. The presence of wide pores bounded by 12-membered rings provides a decrease in diffusion limitation characteristic of medium- and narrow-pore zeolites. On the other hand, according to the authors of [6], zeolite BEA is characterized by the lowest binding energy between a cumene molecule and an active acid site compared with other zeolites. This feature ensures an effective desorption of the target product and providesthe formation of the lowest amount of byproducts.

An analysis of the published data makes it possible to identify key parameters that affect the catalytic properties of zeolite BEA; these parameters are the SiO_2/Al_2O_3 molar ratio, the acidity associated with this ratio, and the zeolite crystal size. However, it should be noted that the number of reports on the effect of these parameters on the catalytic properties of zeolite BEA in benzene alkylation with propylene is extremely scarce; the conclusions in those reports are mostly based on data on cumene synthesis in a batch reactor at a temperature of 150°C and a pressure of about 3 MPa [6, 8]. The cited authors showed that a decrease in the SiO_2/Al_2O_3 ratio in the zeolite from 350 to 20 was accompanied by an increase in the conversion of both benzene (from 2.6 to 12.9% [8]) and propylene (from 40 to 100% [6, 8]); the maximum catalyst activity was achieved at a SiO_2/Al_2O_3 ratio of 28. At the same time, selectivities for cumene and diisopropylbenzenes (DIPBs) varied only slightly. A decrease in the zeolite crystal size from 1 to 0.2 μm led to an increase in propylene conversion and cumene selectivity, while selectivity for polyalkylbenzenes and propylene oligomers decreased [6]. The results obtained by the authors of [6] showed that a decrease in the size of BEA zeolite crystals to a nanoscale is an effective factor that makes it possible to control the catalytic properties of zeolite BEA in benzene alkylation with propylene running in the batch reactor.

This study is focused on the effect of the chemical composition of nanocrystalline zeolites BEA on their physicochemical and catalytic properties in benzene alkylation with propylene in a flow reactor.

EXPERIMENTAL

Nanocrystalline zeolites BEA were synthesized by hydrothermal crystallization from a reaction mixture with the following molar composition: $0.04Na_2O \cdot 0.04K_2O \cdot 0.5(C_2H_5)_4NOH \cdot xAl_2O_3 \cdot SiO_2 \cdot 16H_2O$, where $x = 0.04$, 0.02, 0.01, and 0.005. Precursors were aerosil, sodium aluminate, sodium hydroxide, tetraethylammonium hydroxide, sodium chloride, and potassium chloride. The hydrothermal crystallization and postsynthesis treatments of the synthesized samples were conducted as described in [9]. The synthesized zeolites were designated as BEA-N, where N is the SiO_2/Al_2O_3 molar ratio in the hydrogen form of the sample.

The chemical composition of the samples was studied by X-ray fluorescence analysis on a Thermo Scientific ARL Perform`X instrument with a 3.5-kW rhodium tube.

The phase analysis of the samples was conducted using diffraction patterns recorded on a Bruker D2PHASER X-ray diffractometer using CuK_α radiation. The diffraction patterns were recorded in a 2θ angular range of 4°–80° in increments of 0.09° at a slit width of 1 mm and an acquisition time of 5 s per point.

Characteristics of the porous structure of zeolite BEA were determined by low-temperature nitrogen adsorption–desorption. Isotherms were recorded in accordance with the standard procedure on an ASAP 2010 porosimeter (Micromeritics, United States). The calculation of pore structure characteristics was conducted using the dedicated software.

Scanning electron microscopy (SEM) images of nanocrystalline zeolites BEA were recorded on a Bruker TM 3030 electron microscope. Before recording, a layer of gold was deposited on the sample surface by vacuum deposition. Transmission electron microscopy (TEM) images of zeolites BEA were recorded on a JEOL JEM-2010 electron microscope. Before recording, the samples were placed on a perforated carbon film mounted on a copper grid.

Before determining the acidic and catalytic properties of the zeolites, zeolite powders were compressed into pellets, which were subsequently crushed to obtain a fraction of 0.5 × 1 mm.

The acidic properties of the samples were studied by temperature-programmed desorption of ammonia (NH_3-TPD). Experiments were conducted on a USGA-101 chemisorption analyzer (UNISIT, Russia). The sample in an amount of 0.15–0.20 g was charged into a quartz tube reactor; the standard automatic pretreatment included the following sequential procedures: calcining the sample in a helium stream at 500°C for 1 h, saturation with ammonia at a temperature of 60°C for 15 min, and removal of physically adsorbed ammonia in a helium stream at 100°C. The NH_3-TPD experiment was conducted in a helium stream (30 mL/min) at a rate of temperature increase of 8°C/min; desorbed ammonia was registered using a thermal conductivity detector.

The catalytic properties of the samples in benzene alkylation with propylene were studied in a flow catalytic unit equipped with a fixed-bed reactor a at a pressure of 3 MPa, a temperature of 170°C, a weight hourly space velocity (WHSV) of 25 and 1300 g/(g h), in a nitrogen stream at a flow rate of 30 mL/min, and a benzene/propylene molar ratio of 5/1 and 10/1, respectively. A weighed portion of the catalyst with a fraction of 0.5–1 mm diluted with quartz with a fraction of 1–2 mm was loaded into the reactor which was placed in an oven. The temperature of the reaction zone was controlled using a chromel–alumel thermocouple located in the catalyst bed. A benzene–propylene mixture was fed into the reactor by means of a piston pump. Prior to feeding the reaction feedstock, all the catalysts were subjected to conditioning at 350°C in a nitrogen stream at a flow rate of 30 mL/min for 30 min; after that, the temperature was decreased to the reaction temperature.

Gaseous and liquid reaction products were analyzed on Kristall-2000M liquid chromatographs (Khromatek Analitik) equipped with flame ionization detectors using quartz capillary columns coated with the SE-30 phase (30 m). Nitrogen was used as a carrier gas. In the analysis of gas samples, methane was used as an internal standard.

RESULTS AND DISCUSSION

To study effect of the composition of nanocrystalline zeolites BEA on their physicochemical and catalytic properties, a set of samples was synthesized; the characteristics of the samples are listed in Table 1. The selected synthesis conditions provided the formation of highly crystalline samples in which zeolite BEA was present as the only crystalline phase. Analysis of the chemical composition of the synthesized samples showed that, in all samples, the SiO_2/Al_2O_3 ratio is significantly lower than that in the feed reaction mixture; this fact suggests that silicon introduced into the initial gel is incompletely involved in the zeolite composition. With an increase in the SiO_2/Al_2O_3 ratio in the reaction mixture (25, 50, 100, and 200), the degree of involvement of silicon in the zeolite decreased; the SiO_2/Al_2O_3 ratios in the samples were 14, 21, 32, and 55, respectively. A change in the chemical composition of the zeolite was accompanied by morphological changes. The BEA-14 sample with $SiO_2/Al_2O_3 = 14$ was represented by nanocrystals with a size of about 100 nm which were combined into aggregates with a size of 1.0–1.5 μm (Fig. 1a). A decrease in aluminum

Table 1. Morphological and textural characteristics of nanocrystalline zeolites BEA

Sample	Morphology and size of crystals	Pore volume, cm^3/g	Micropore volume, cm^3/g	Micropore surface area, m^2/g	Exteenal surface area, m^2/g
BEA-14	Aggregates with a size of 1.0–1.5 μm composed of 100-nm nanocrystals	0.23	0.18	350	100
BEA-21	Aggregates with a size of 150–300 nm composed of nanocrystals with a size of 10–30 nm	0.32	0.19	410	160
BEA-32	Aggregates with a size of 200–300 nm composed of nanocrystals with a size of 20–30 nm	0.33	0.23	490	125
BEA-55	Cylindrical nanocrystals with a size of 250–300 nm	0.32	0.24	530	85

concentration in the reaction mixture during the synthesis of the BEA-21 and BEA-32 samples led to the formation of nanoaggregates composed of primary nanocrystallites (Figs. 1b, 1c; Table 1). A further decrease in the aluminum content in the BEA-55 sample led to the formation of isolated nanocrystals (Fig. 1d) with a narrow particle size distribution (Table 1).

The textural properties of nanocrystalline zeolites BEA were studied by low-temperature nitrogen adsorption (Fig. 2). The pore structure characteristics calculated according to the isotherms are listed in Table 1. The isotherm of the BEA-14 sample fully corresponds to the type I isotherm according to the IUPAC classification; this fact suggests that the sample is microporous. The high external surface area of this sample, which is 100 m^2/g (Table 1), corresponds to the aggregative form of zeolite nanocrystals (Fig. 1a). A decrease in the size of the primary nanocrystals in the BEA-21 and BEA-32 samples led to an

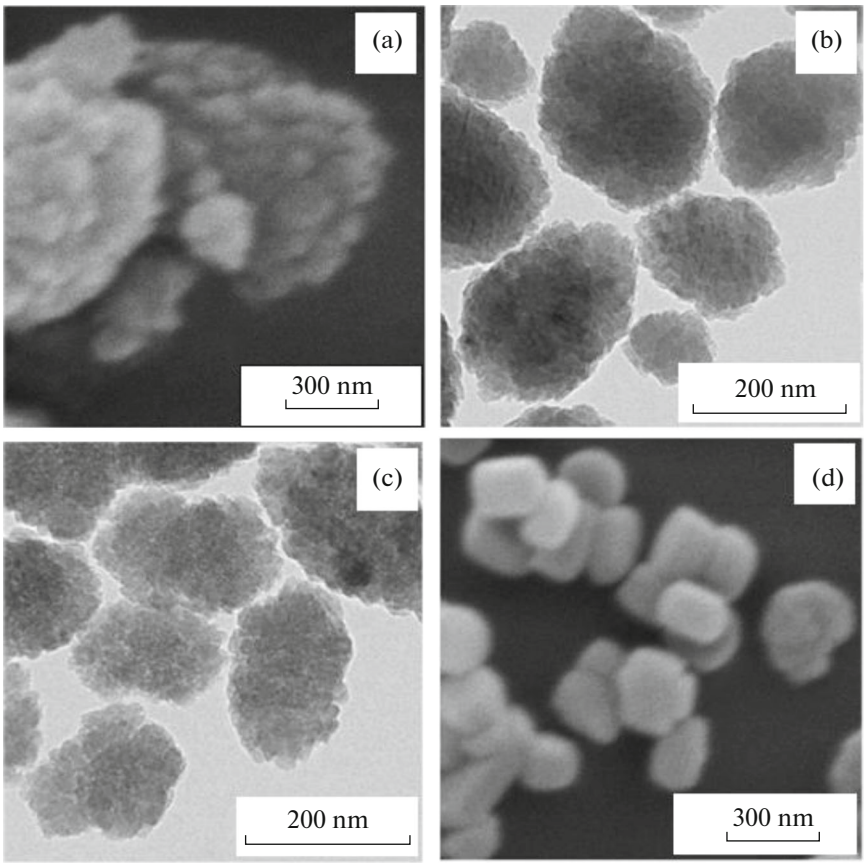

Fig. 1. (a, d) SEM and (b, c) TEM micrographs of nanocrystalline zeolites BEA: (a) BEA-14, (b) BEA-21, (c) BEA-32, and (d) BEA-5.5.

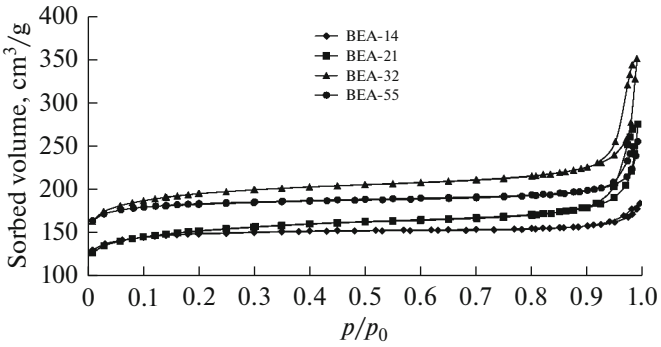

Fig. 2. Low-temperature nitrogen adsorption–desorption isotherms for zeolites with different SiO_2/Al_2O_3 ratios.

increase in the external surface area to 160 and 125 m^2/g, respectively (Table 1). The isotherms of these samples exhibit abruptly ascending portions in the region of p/p_0 values of 0.9–0.95, which indicates the presence of mesopores. Apparently, mesopores in these nanocrystalline materials are formed at the point contacts of primary nanocrystals with a size of 10–30 nm in nanoagglomerates. A similar ascending portion is observed in the isotherm of the BEA-55 sample; however, compared to the isotherms of the BEA-21 and BEA-32 samples, the position of this portion is shifted to the region of higher p/p_0 values. This shape of the isotherm is typical of nanocrystalline zeolites with isolated crystals. The formation of individual crystals with a size of 250–300 nm led to a decrease in the external surface area of this sample to 85 m^2/g (Table 1).

The acidic properties of the samples were studied by the NH_3-TPD method (Table 2, Fig. 3). The NH_3-TPD curves exhibit two peaks indicating the presence of two types of acid sites, namely, weak sites with a thermal desorption maximum at 200–230°C and strong sites with a thermal desorption maximum at 350–420°C (Fig. 3). The acid site concentrations $a_0(NH_3)$ and densities $d_0(NH_3)$ in nanocrystalline zeolites BEA correlated with the aluminum content in the samples (Table 2). With a decrease in the SiO_2/Al_2O_3 ratio from 55 to 14 and a respective increase in the aluminum concentration in the zeolites, the $a_0(NH_3)$ value increased from 750 to 1430 μmol/g. Since the high-temperature maxima in the TPD spectra have identical intensities (Fig. 3), it can be assumed that the BEA-21 and BEA-14 samples have approximately identical concentrations of strong acid sites, and differences in the acid site concentrations (1430 and 1350 μmol/g, respectively) are mostly associated with the content of weak acid sites in the samples. For the BEA-32 and BEA-55 samples, the position of the high-temperature maximum is shifted toward lower temperatures; this shift can indicate a decrease in the strength of the acid sites in these samples.

The catalytic properties of nanocrystalline zeolites BEA were studied in benzene alkylation with propylene at a temperature of 170°C and a pressure of 3 MPa (Tables 3, 4). Two modes were selected for catalytic tests. The first mode involved implementation of the process at WHSV = 1300 g/(g h) and benzene/propylene = 10/1. This mode made it possible to correctly compare the activity of the nanocrystalline zeolites at a decreased propylene conversion of 68–82%.

According to the results of catalytic conversions (Table 3), the main reaction products were cumene and DIPB; negligible amounts of triisopropylbenzene (TIPB), *n*-propylbenzene, propylene oligomers, and alkylaromatic hydrocarbons were observed. The highest activity of all the nanocrystalline zeolite samples was exhibited by the BEA-21 sample, which provided a propylene conversion of 82.3%. Comparison of the results of the catalytic action of the BEA-14 and BEA-21 samples suggests the following. The BEA-14 sample was inferior in activity to the BEA-21 sample, although the acid site concentration and density for

Table 2. Acidic properties of nanocrystalline zeolites BEA

Sample	Aluminum concentration, μmol/g	Acid site concentration $a_0(NH_3)$, μmol/g	Acid site density $d_0(NH_3)$, μmol/m^2
BEA-14	2120	1430	3.2
BEA-21	1470	1350	2.4
BEA-32	990	1110	1.8
BEA-55	590	750	1.2

the former were higher (with close micropore volumes), as evidenced by Tables 1 and 2. Apparently, the advantages of the BEA-21 sample in this on-stream mode of the catalyst are attributed to morphological features rather than to acidic properties. This sample has the most developed external surface (160 m^2/g) owing to the size of the nanocrystallites (10–30 nm) that constitute nanoaggregates (Table 1). This morphology of particles provides a higher accessibility of the reacting molecules to the acid sites of the zeolite and, thereby, a high activity of the sample. The activity of the BEA-14 sample, which is lower than that of the BEA-21 sample, determined its selective properties, namely, a higher cumene selectivity and a lower selectivity for DIPB and TIPB (Table 3). The BEA-32 and BEA-55 samples exhibited a lower propylene conversion, which correlates with the NH_3-TPD data.

For all the samples, the cumene selectivity was higher than 90% (Table 3). The highest cumene selectivities (93.5 and 92.7 wt %) were observed for the BEA-14 and BEA-21 samples; this fact can be explained by a higher acid site concentration in these catalysts, which provides a decrease in the contribution of secondary processes. A decrease in the acid site concentration in the BEA-21 sample (1350 μmol/g) compared with the respective parameter of BEA-14 (1430 μmol/g) led to a slight decrease in cumene selectivity and an increase in selectivity for DIPB and TIPB. The BEA-55 sample ensured formation of the largest amount of propylene oligomers (0.11 wt %), which caused the rapid deactivation of this catalyst owing to the consecutive occurrence of olefin oligomerization, cyclization, and aromatization.

The second mode of catalytic testing was similar to the industrial on-stream conditions of the catalysts providing 100% propylene conversion. This mode involved a decrease in WHSV to 25 g/(g h) and benzene/propylene molar ratio to 5 : 1. These process conditions made it possible to compare selectivities for reaction products.

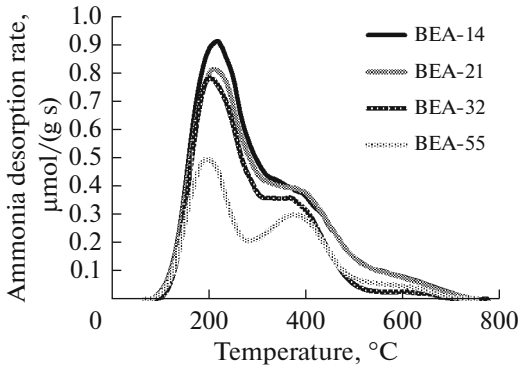

Fig. 3. Ammonia TPD spectra of the samples.

Against the background of identical catalytic activity of all the zeolites (nearly 100% propylene conversion), the highest cumene selectivity and cumene yield were provided by the BEA-14 sample (Table 4). In addition, the BEA-14 sample was characterized by a lower yield of secondary alkylation products (DIPB and TIPB). Thus, in the 100% propylene conversion mode, the advantages of the BEA-21 sample associated with the developed external surface and the extremely small size of nanocrystallites are neutralized; a more important parameter responsible for the catalytic properties of zeolite BEA becomes its acidity. The formation of a lower amount of polyalkyl derivatives in the presence of the BEA-14 sample can be attributed to a higher acid site concentration. The BEA-21 and BEA-32 samples were characterized by similar selectivities for cumene, DIPB, and TIPB. The lowest cumene yield was observed for the BEA-55 sample; compared with other samples, this catalyst provided the formation of the largest amount of *n*-propylbenzene and an increased amount of polyalkyl derivatives and propylene oligomers (Table 4).

Thus, it has been found that the key factor responsible for the catalytic properties of zeolites in benzene

Table 3. Catalytic properties of nanocrystalline zeolites BEA in benzene alkylation with propylene (WHSV = 1300 g/(g h), P = 3 MPa, T = 170°C, benzene/propylene = 10/1 mol/mol)

Process parameters	Catalyst			
	BEA-14	BEA-21	BEA-32	BEA-55
Conversion of C_3H_6	78.2	82.3	76.3	67.7
Product selectivity, wt %				
Cumene	93.5	92.7	90.9	90.6
DIPB	6.5	7.2	8.9	9.2
TIPB	0	0.02	0.07	0.09
n-Propylbenzene	0.03	0.03	0.03	0.03
Propylene oligomers and alkylaromatic hydrocarbons	0.06	0.07	0.07	0.11
Cumene yield, %	73	76.3	69.4	61.3

Table 4. Catalytic properties of nanocrystalline zeolites BEA in benzene alkylation with propylene (WHSV = 25 g/(g h), P = 3 MPa, T = 170°C, and benzene/propylene = 5/1 mol/mol)

Process parameters	Catalyst			
	BEA-14	BEA-21	BEA-32	BEA-55
Conversion of C_3H_6	99.9	99.9	99.9	99.9
Product selectivity, wt %				
Cumene	88	84.8	84.3	82.3
DIPB	11.5	14.7	15.1	16.7
TIPB	0.08	0.14	0.17	0.37
n-Propylbenzene	0.03	0.03	0.04	0.05
Propylene oligomers and alkylaromatic hydrocarbons	0.35	0.33	0.37	0.6
Cumene yield, %	87.7	84.8	84.3	82.3

alkylation with propylene is the catalyst acidity. It has been shown that the highest zeolite activity and selectivity for the target product—cumene—are provided by the combination of the acidic and morphological characteristics of nanocrystalline zeolites BEA.

FUNDING

This work was performed under the State Task for the Topchiev Institute of Petrochemical Synthesis, Russian Academy of Sciences.

CONFLICT OF INTEREST

The authors declare that there is no conflict of interest regarding the publication of this manuscript.

ADDITIONAL INFORMATION

E.P. Andriako, ORCID: https://orcid.org/0000-0002-8074-424X

T.O. Bok, ORCID: https://orcid.org/0000-0002-7882-5833

D.O. Bachurina, ORCID: https://orcid.org/0000-0001-5032-6381

E.E. Knyazeva, ORCID https://orcid.org/0000-0002-6944-174X

I.I. Ivanova, ORCID: https://orcid.org/0000-0002-8742-2892

REFERENCES

1. J. P. Fortuin and H. I. Waterman, Chem. Eng. Sci. **2**, 182 (1953).
2. V. M. Zakoshanskii, Pet. Chem. **47** (4), 273 (2007).
3. E. K. Jones and D. D. Dettner, U.S. Patent No. 2 860 173 (1958).
4. T. F. Degnan, C. M. Smith, and C. R. Venkat, Appl. Catal., A **221**, 283 (2001).
5. A. V. Smirnov, B. V. Romanovsky, I. I. Ivanova, E. G. Derouane, and Z. Gabelica, Stud. Surf. Sci. Catal. **84**, 1797 (1994).
6. C. Perego, S. Amarilli, R. Millini, G. Bellussi, G. Girotti, and G. Terzoni, Microporous Mater. **6**, 395 (1996).
7. A. Corma, V. Martinez-Soria, and E. Schnoeveld, J. Catal. **192** (1), 163 (2000).
8. H. Wang and W. Xin, Catal. Lett. **76** (3–4), 225 (2001).
9. T. O. Bok, E. D. Onuchin, A. V. Zabil'skaya, S. V. Konnov, E. E. Knyazeva, A. V. Panov, A. V. Kleimenov, and I. I. Ivanova, Pet. Chem. **56** (12), 1160 (2016).

Translated by M. Timoshinina